Constraint on a Varying Proton-Electron Mass Ratio 1.5 Billion Years after the Big Bang

J. Bagdonaite and W. Ubachs
Department of Physics and Astronomy, and LaserLaB, VU University, De Boelelaan 1081, 1081 HV Amsterdam, Netherlands

M. T. Murphy and J. B. Whitmore
Centre for Astrophysics and Supercomputing, Swinburne University of Technology, Melbourne, Victoria 3122, Australia
(Received 31 October 2014; revised manuscript received 15 January 2015; published 19 February 2015)

A molecular hydrogen absorber at a lookback time of 12.4 billion years, corresponding to 10% of the age of the Universe today, is analyzed to put a constraint on a varying proton-electron mass ratio, μ. A high resolution spectrum of the J1443+2724 quasar, which was observed with the Very Large Telescope, is used to create an accurate model of 89 Lyman and Werner band transitions whose relative frequencies are sensitive to μ, yielding a limit on the relative deviation from the current laboratory value of $\Delta\mu/\mu = (-9.5 \pm 5.4_{\mathrm{stat}} \pm 5.3_{\mathrm{syst}}) \times 10^{-6}$.

DOI: 10.1103/PhysRevLett.114.071301 PACS numbers: 98.80.-k, 06.20.Jr, 33.20.-t, 98.58.-w

The accelerated expansion of the Universe is ascribed to an elusive form of gravitational repulsive action referred to as dark energy [1]. Whether it is a cosmological constant, inherent to the fabric of space-time, or whether it may be ascribed to some dynamical action in the form of a scalar field ϕ [2], is an open issue. In the latter case it has been shown that the interaction of the postulated quintessence fields ϕ to matter cannot be ignored, giving rise to a variation of the fundamental coupling constants and a breakdown of the equivalence principle [3,4]. In this context it is particularly interesting to probe possible variations of the fundamental constants in the cosmological epoch of the phase transition, going from a matter-dominated universe to a dark energy-dominated universe, covering redshift ranges $z = 0.5 - 5$ [5]. While models of big bang nuclear synthesis probe fundamental constants at extremely high redshifts ($z = 10^8$) [6], the Oklo phenomenon ($z = 0.14$) [7] and laboratory atomic clock experiments ($z = 0$) [8] probe low redshifts. Absorbing galaxies in the line-of-sight of quasars are particularly suitable for investigating the range of medium-high redshifts, for a varying fine-structure constant, α, based on metal absorption [9] and for a varying proton-electron mass ratio, $\mu = m_p/m_e$, based on molecular absorption [10]. Furthermore, unification scenarios predict that variations of α and μ are connected, while in most schemes μ is a more sensitive target for varying constants [11].

A variation of μ may be probed through the spectroscopy of molecules such as hydrogen (H_2) [12], ammonia (NH_3) [13], and methanol (CH_3OH) [14]. The latter polyatomic molecules are more sensitive to a variation in μ under the assumption that molecular reduced masses, involving protons and neutrons, scale in a similar manner as μ, which can be probed in a pure form in H_2 [10]. Moreover, the radio absorption systems, where the polyatomic absorbers can be found, are more rare and are currently only found at the lower redshifts $z = 0.68$ [15,16] and $z = 0.89$ [14]. Molecular lines observed at $z = 6.34$ [17] are of insufficient spectral quality to constrain μ variation. Conveniently, the ultraviolet spectrum of the H_2 Lyman and Werner bands can be investigated with large ground-based optical telescopes for absorbers at redshifts $z > 2$. The current sample of H_2-based measurements covers a redshift interval from 2 to 3 [18,19], with the highest redshift object Q0347–383 at $z = 3.025$ [20,21].

Here we constrain variations in μ at substantially higher redshift by analyzing an H_2 absorber at $z = 4.22$ along the sight line towards the background ($z = 4.42$) quasar PSSJ1443+2724 [22]. This step to higher redshift is challenging for several reasons. First, more distant quasars are typically fainter, making initial discovery of the H_2 absorption more difficult and requiring longer integration times for a high-quality spectrum with which to constrain $\Delta\mu/\mu$. Second, absorption lines from neutral hydrogen (HI) in the intergalactic medium are more numerous at higher redshifts, complicating analysis of the H_2 transitions. The Lyman-series transitions from the many unrelated HI clouds in the intergalactic medium form a characteristic "forest" of broader spectral features against which the H_2 have to be identified and analyzed (see Fig. 1). However, the "comprehensive fitting" method of simultaneously treating this HI forest and the H_2 absorption, developed previously and documented extensively [18,20,23,24], is employed here to reliably meet this challenge.

A portion of the J1443+2724 spectrum is shown in Fig. 1. To create the spectrum, we make use of an archival data set obtained in 2004 [22] and a new data set obtained in 2013 (Program ID 090.A-0304) which comprise, respectively, 7.3 and 16.7 h (5 and 12 exposures) observation time with the Very Large Telescope/the Ultraviolet and Visual Echelle Spectrograph (VLT/UVES). For weak light sources as the present quasar (visual magnitude $V \sim 19.4$) long integration time is required to reach signal-to-noise ratio

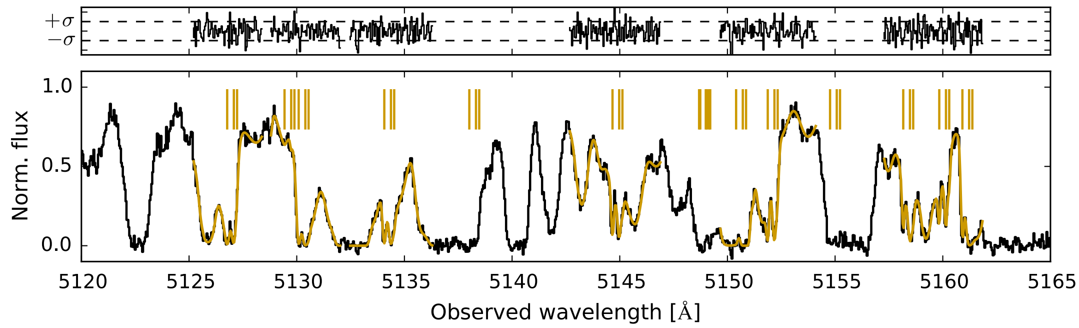

FIG. 1 (color online). Part of the final, fitted spectrum of J1443+2724. The sticks indicate the 3 velocity components of each H_2 transition. The residuals are shown above the spectrum for the regions fitted. The broad features that surround and overlap the fitted H_2 transitions are multiple, unrelated H I absorption lines arising in other absorbers along the line of sight.

(SNR) of > 30, especially if high spectral resolution is required. Wavelength calibration in the UVES instrument is achieved by observing a reference ThAr lamp. After each night of observations (in 2004) or, preferably, immediately after each quasar exposure (in 2013) a spectrum of the ThAr lamp was recorded using identical settings to those of the science exposure. The ThAr spectrum was used by the UVES data-reduction pipeline to create pixel-vs-wavelength maps and apply them to the quasar exposures. The wavelength scales of the spectra were converted to vacuum-heliocentric values. Following the same procedures as in [18,23,24], flux-extracted individual exposures were then resampled, scaled, and merged to a final 1D spectrum that extends from 474 to 792 nm, with the H_2 transitions detected at 484–581 nm. The SNR at shorter wavelengths is entirely dominated by the data from 2004 as the observations in 2013 were affected by stray light from the full moon.

As shown in Fig. 2, each H_2 transition in the J1443+2724 spectrum has two distinct velocity features. In the comprehensive fitting method employed here, these two features in all H_2 transitions are fitted simultaneously (along with the many broader, unrelated H I forest features). With this approach, one makes use of the known molecular physics of H_2, thereby reducing the number of free parameters in the fit. In particular, transitions from the same ground rotational level J are fitted using a single parameter for column density N_J, while for the same velocity component (VC), transitions from all J levels are tied in terms of redshift z and linewidth b. The intrinsic intensities of the H_2 absorbing transitions are fixed to the oscillator strengths known from the molecular physics database [23]. In this way, the best fit is achieved by simultaneously combining information from multiple spectral regions. In the case of J1443+2724, we selected 60 spectral regions containing a total of 89 H_2 transitions up to $J = 4$, among which 17 are from the Werner band [25]. This approach, along with the simultaneous fitting of the H I forest lines, is the same as detailed previously (e.g., [18,24]). The χ^2 minimization is performed using a Voigt profile fitting program VPFIT9.5 [26]. To fit each transition i, a Voigt profile is created from a threefold convolution of a Lorentzian profile defined via a damping parameter Γ_i, a Gaussian profile describing the thermal and turbulent velocities in the gas, and an instrumental profile. For the ith transition of H_2 detected at redshift $z_{\rm abs}$, the recorded wavelength is expressed as

$$\lambda_i = \lambda_i^0 (1 + z_{\rm abs}) \left(1 + K_i \frac{\Delta\mu}{\mu}\right), \tag{1}$$

where λ_i^0 is the corresponding laboratory wavelength, and K_i is a coefficient that quantifies the sign and magnitude of its sensitivity to a varying μ [12], and where that variation is parametrized by $\Delta\mu/\mu = (\mu_z - \mu_{\rm lab})/\mu_{\rm lab}$.

The two velocity features per transition can contribute towards better precision of $\Delta\mu/\mu$. However, previous studies have shown that an inadequate fit of H_2 features can produce a spurious $\Delta\mu/\mu$ value [27]. In particular, underfitted velocity profiles are more prone to such errors. To avoid that, additional VCs are included in the profile

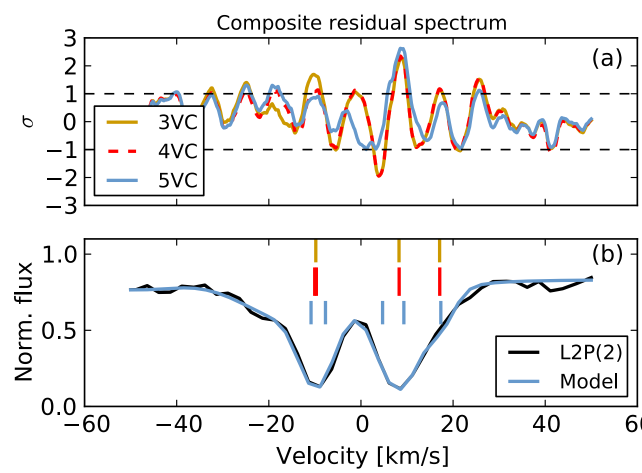

FIG. 2 (color online). (a) Composite residual spectra of 31 transitions shown for the 3, 4, and 5 VC models. (b) A H_2 absorption profile in the J1443+2724 spectrum. The sticks indicate the positions of velocity components for the 3, 4, and 5 VC models.

TABLE I. Results of fitting models of increasing complexity to the spectrum. The two velocity features (see Fig. 2) require fitting at least 2 velocity components (VC); but as it can be seen from the goodness-of-fit measure χ^2_ν (where ν is the number of degrees of freedom; here $\nu \sim 4600$) models with 3, 4, and 5 VC replicate the data better. For each model, a resulting $\Delta\mu/\mu$ value is shown in the last column.

Number of VCs	χ^2_ν	$\Delta\mu/\mu$ [$\times 10^{-6}$]
2	1.396	-8.7 ± 5.2
3	1.161	-6.7 ± 5.4
4	1.139	-8.3 ± 5.4
5	1.133	-2.9 ± 5.2

to check for a more complex velocity structure than can be appreciated by eye. The additional components can be rejected by VPFIT as statistically unjustified or they can remain and improve the model. Table I contains the results of fitting increasingly complex models to the H_2 spectrum of J1443+2724. Figure 2 displays composite residual spectra of different models. The composite residual spectra are created by combining a number of residuals of individual transitions, which are aligned in velocity or redshift space [23]. While according to the reduced χ^2 value, a model with 4 or 5 VCs initially might appear preferable to one with only 3 VCs, fitting the former more complex models was not stable: VPFIT rejected the additional VCs in lower-J transitions while retaining them in higher-J transitions, thereby departing from a physically plausible, self-consistent model. Figure 2 shows that adding a second VC to the left feature of the absorption profile reduces the composite residuals, but that the residuals for the right feature are barely affected when adding a third VC.

In all the models, the H_2 absorption feature on the right requires fitting of at least one very narrow component. This weak component exhibits an unusually high relative column density for $J = 2, 3$ levels, and a width of 0.2 km/s, corresponding to a kinetic temperature of 5 K, hence lower than $T_{\rm CMB} = 14$ K at $z = 4.22$. While this low b value results from a best-fit model and hence is favored statistically, we performed further testing by imposing $b_{\rm min}$ parameters corresponding to temperatures including those in the expected kinetic regime of 50–100 K ($b \sim 0.6$–0.9 km/s). These tests, performed for 3 and 4 VC models demonstrate that resulting values for $\Delta\mu/\mu$ do not critically depend on the narrowness of this velocity feature [28]. A spectrum of a higher SNR and higher resolution might help in explaining the composite residual excess and the N, b values obtained here.

TABLE II. Results of fitting a 3 VC model to the data.

$z_{\rm abs}$	b [km/s]	$\log N \pm \sigma_{\log N}$ from $J = 0$ to $J = 4$
4.223 729 2(6)	1.74 ± 0.06	17.04 ± 0.06, 17.40 ± 0.05, 15.86 ± 0.09, 14.81 ± 0.04, 12.99 ± 0.84
4.224 044 0(11)	0.42 ± 0.18	17.49 ± 0.03, 17.87 ± 0.02, 17.34 ± 0.02, 17.09 ± 0.03, 13.80 ± 0.33
4.224 197 5(20)	0.20 ± 0.08	15.01 ± 0.33, 16.17 ± 0.10, 15.77 ± 0.09, 15.97 ± 0.06, 13.67 ± 0.61

Based on the internal consistency of various fitting results, a model with 3 VCs is selected as the fiducial model (see Table II for fitting results) and is further tested for possible systematics. The 4 and 5 VC fits are used to verify the results of the fiducial model.

The fiducial 3 VC model delivers $\Delta\mu/\mu = (-6.7 \pm 5.4_{\rm stat}) \times 10^{-6}$. Figure 3 shows how this result compares to constraints obtained from fitting only certain selected transitions, velocity components, or parts of the spectrum. Most of the derived constraints are compatible with the fiducial result, demonstrating that the result is robust. Nevertheless, a possible discrepancy is that constraints from the low- and high-J transitions seem to move in opposite directions if fitted separately. This tendency is observed in the 4 and 5 VC models as well. If the redshift and width parameters are tied separately for the low-J and high-J transitions the resulting z and b parameter values agree well between the two groups. Fitting only the small number of Werner transitions (17), together with their smaller spread in K_i coefficients, results in a large uncertainty in $\Delta\mu/\mu$. Fitting a spectrum that includes only the exposures from 2004 delivers $\Delta\mu/\mu = (-0.2 \pm 6.4_{\rm stat}) \times 10^{-6}$. This constraint, as well as the constraints derived from the 4 and 5 VC models on a full spectrum, are in agreement with the result from the fiducial model. Fitting a spectrum that includes only 2013 exposures results in $\Delta\mu/\mu = (4.0 \pm 12.4_{\rm stat}) \times 10^{-6}$.

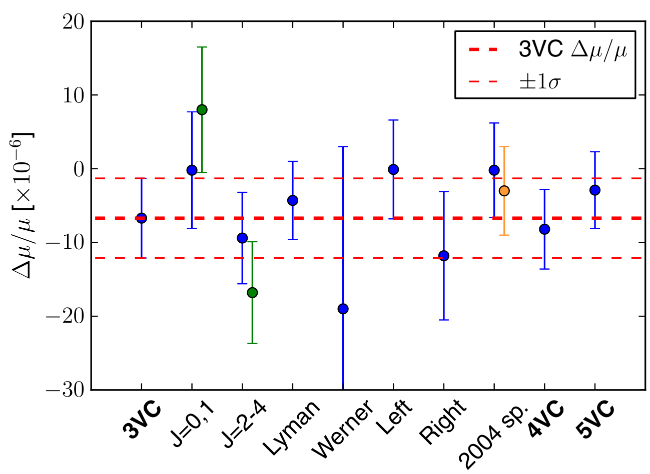

FIG. 3 (color online). Statistical $\Delta\mu/\mu$ constraints obtained from the fiducial 3 VC model, from various tests performed on it, and from the 4 and 5 VC models. The green points refer to fitting low- and high-J transitions with the z and b parameters tied within each group but not between the two groups. The left and the right tests refer to deriving $\Delta\mu/\mu$ constraints from the two velocity features of H_2 separately (see Fig. 2). The orange point was obtained after the spectrum obtained in 2004 has been corrected for long-range wavelength distortions.

The uncertainty is much larger because the SNR of the data collected in 2013 is affected by additional noise from the full moon.

The accuracy to which $\Delta\mu/\mu$ can be measured strongly relies on accurate wavelength calibration of the quasar spectrum. At any wavelength in the J1443+2724 spectrum, the error of the wavelength calibration solution is ~70 m/s which translates to $\Delta\mu/\mu$ of 1×10^{-6} given a spread in K_i coefficients of 0.05 [29].

An additional source of systematic uncertainty might be caused by wavelength-scale distortions inherent to the instrument. Short-range distortions with a characteristic shape repeating in each diffraction order of the echelle spectrograph were found in UVES [30]. We estimate its potential to systematically shift the $\Delta\mu/\mu$ value by applying a sawtooth-like distortion of ±100 m/s to each order and fitting the recombined spectrum, as in [23,24]. This results in a $\Delta\mu/\mu$ shift as small as 1×10^{-7}.

Recently, indications were reported that the UVES instrument is also susceptible to long-range wavelength distortions that are able to mimic nonzero $\Delta\mu/\mu$ values at the level of several parts per million [19]. Their origin is not clear but deviations between the light paths of the quasar and ThAr lamp are considered the likely (proximate) cause. The effect of such a miscalibration can be quantified by observing objects that have well-understood spectra, such as asteroids which reflect the solar spectrum and stars with solarlike spectra, known as solar twins [19,24,31,32]. In the archive of UVES [33] we found several sunlike stars that were observed in 2004, at a similar time as the J1443+2724 quasar [34]. By comparing their spectra to a highly accurate Fourier-transform spectrum of the Sun [35], we found a correction amounting to 44.9 ± 46.8 m/s/1000 Å. An extensive study of this particular systematic effect shows that corrections of this size are typical for the considered time period [32]. Applying the aforementioned correction on the wavelength scale of the spectrum obtained in 2004 results in a $\Delta\mu/\mu$ shift of -2.8×10^{-6} if compared to the uncorrected constraint. The uncertainty on this correction translates into a systematic $\Delta\mu/\mu$ uncertainty of 1.6×10^{-6}. We consider this shift a representative correction for the long-range wavelength distortions of the total spectrum since 84% of the fiducial $\Delta\mu/\mu$ accuracy is gained from the 2004 exposures.

Creating a 1D spectrum from multiple exposures and overlapping echelle orders involves redispersion onto a single wavelength grid. The rebinning causes correlation in flux and flux uncertainty values between adjacent pixels. Varying the dispersion bin size from the default value of 2.5 km/s by ±0.1 km/s results in an average $\Delta\mu/\mu$ shift of $\pm 4 \times 10^{-6}$.

The spectra were obtained using 1.0 and 0.8″ slit widths in 2004 and 2013, respectively. This corresponds to respective spectral resolutions of $R \sim 38700$ and ~48500 or Gaussian instrumental profiles with the width of $\sigma_{\rm inst} =$ 3.3 and 2.6 km/s. However, the profile to be convolved

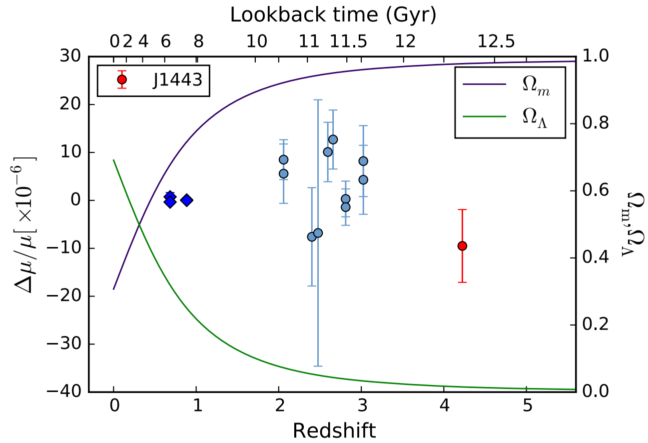

FIG. 4 (color online). The nonrelativistic mass density parameter Ω_m and the dark energy density parameter Ω_Λ as functions of redshift, with a corresponding lookback time axis on top. Results from various $\Delta\mu/\mu$ studies: the diamond markers refer to the measurements of rotational transitions of methanol and ammonia [13–16], while $\Delta\mu/\mu$ values derived from H_2 observations are denoted by circles [18–21,23,24,38,39].

with the fitted line profile will be up to ~10% narrower because the quasar light is concentrated towards the center of the slit. The fiducial $\Delta\mu/\mu$ constraint was derived from the combined 2004 and 2013 spectra using an instrumental profile of $\sigma_{\rm inst} = 2.6$ km/s. Varying the $\sigma_{\rm inst}$ in the range from 2.6 to 2.9 km/s resulted in deviations from the fiducial $\Delta\mu/\mu$ constraint as large as 3×10^{-6}.

In summary, the constraint on $\Delta\mu/\mu$ derived from this quasar spectrum shows sensitivity to these systematic effects. All the contributions combined (added in quadrature) constitute the total systematic error budget of $\sigma_{\rm syst} = 5.3 \times 10^{-6}$. After correction for the long-range wavelength distortions, our fiducial constraint therefore becomes $\Delta\mu/\mu = (-9.5 \pm 5.4_{\rm stat} \pm 5.3_{\rm syst}) \times 10^{-6}$.

This result constrains a possible variation of the proton-electron mass ratio by means of the H_2 spectroscopic method for the highest redshift so far. Figure 4 displays a comparison with previous data, mainly showing results derived from H_2 absorbers toward quasars in the redshift interval $z = 2$–3, as well as the more constraining results from radio astronomy of polyatomic molecules for $z < 0.9$. With the analysis of the absorber toward J1443+2724 the window $z > 4$ is opened. A further comparison can be made with a result from radio astronomy of a lensed galaxy probing a (7–6) rotational transition in CO and a fine-structure transition in atomic carbon ($^3P_2 - {}^3P_1$) at $z =$ 5.2 corresponding to 12.7 Gyr lookback time [36]; that study probes the combination of dimensionless constants $F = \alpha^2/\mu$ and yields $\Delta F/F < 2 \times 10^{-5}$ [37].

The presented H_2 constraint signifies a null result. It will assist in setting boundaries to various theories describing physics beyond the standard model [4,5], as well as on the

ΛCDM standard model of cosmology [40]. The densities of matter (including dark matter) Ω_m and dark energy Ω_Λ, and their ratio (see Fig. 4) are important parameters in the models [3], and the present work covers a wide set of values: in the interval $z = 0$–4.22 dark energy covers $\Omega_\Lambda = 0.68$ to 0.015. While a number of cosmological scenarios suggest varying constants [5,11] no quantification of the rate of change is predicted, except for some model-dependent scenarios involving screening and not holding for cosmological time scales [41]. Thus, while a clear threshold for new physics is lacking, the observational and experimental targets are positioned to set ever tighter constraints on varying constants. The present study pushes a tight constraint on a varying μ to lookback times of 10% of the age of the Universe today.

The authors thank the Netherlands Foundation for Fundamental Research of Matter (FOM) for financial support. M. T. M. and J. B. W. thank the Australian Research Council for Discovery Project Grant No. DP110100866, which supported this work. The work is based on observations with the ESO Very Large Telescope at Paranal (Chile).

[1] S. Perlmutter, Nobel Lecture: Measuring the acceleration of the cosmic expansion using supernovae, Rev. Mod. Phys. **84**, 1127 (2012); B. P. Schmidt, Nobel Lecture: Accelerating expansion of the Universe through observations of distant supernovae, Rev. Mod. Phys. **84**, 1151 (2012); A. G. Riess, Nobel Lecture: My path to the accelerating Universe, Rev. Mod. Phys. **84**, 1165 (2012).

[2] B. Ratra and P. J. E. Peebles, Cosmological consequences of a rolling homogeneous scalar field, Phys. Rev. D **37**, 3406 (1988).

[3] S. M. Carroll, Quintessence and the Rest of the World: Suppressing Long-Range Interactions, Phys. Rev. Lett. **81**, 3067 (1998).

[4] J. D. Bekenstein, Fine-structure constant variability, equivalence principle, and cosmology, Phys. Rev. D **66**, 123514 (2002).

[5] H. B. Sandvik, J. D. Barrow, and J. Magueijo, A Simple Cosmology with a Varying Fine Structure Constant, Phys. Rev. Lett. **88**, 031302 (2002).

[6] J. C. Berengut, E. Epelbaum, V. V. Flambaum, C. Hanhart, U.-G. Meißner, J. Nebreda, and J. R. Peláez, Varying the light quark mass: Impact on the nuclear force and big bang nucleosynthesis, Phys. Rev. D **87**, 085018 (2013).

[7] T. Damour and F. Dyson, The Oklo bound on the time variation of the fine-structure constant revisited, Nucl. Phys. **B480**, 37 (1996).

[8] T. Rosenband, D. B. Hume, P. O. Schmidt, C. W. Chou, A. Brusch, L. Lorini, W. H. Oskay, R. E. Drullinger, T. M. Fortier, J. E. Stalnaker, S. A. Diddams, W. C. Swann, N. R. Newbury, W. M. Itano, D. J. Wineland, and J. C. Bergquist, Frequency ratio of Al^+ and Hg^+ single-ion optical clocks; Metrology at the 17th decimal place, Science **319**, 1808 (2008).

[9] M. T. Murphy, J. K. Webb, and V. V. Flambaum, Further evidence for a variable fine-structure constant from Keck/HIRES QSO absorption spectra, Mon. Not. R. Astron. Soc. **345**, 609 (2003).

[10] P. Jansen, H. L. Bethlem, and W. Ubachs, Perspective: Tipping the scales: Search for drifting constants from molecular spectra, J. Chem. Phys. **140**, 010901 (2014).

[11] M. C. Ferreira, O. Frigola, C. J. A. P. Martins, A. M. R. V. L. Monteiro, and J. Solà, Consistency tests of the stability of fundamental couplings and unification scenarios, Phys. Rev. D **89**, 083011 (2014).

[12] W. Ubachs, R. Buning, K. S. E. Eikema, and E. Reinhold, On a possible variation of the proton-to-electron mass ratio: H_2 spectra in the line of sight of high-redshift quasars and in the laboratory, J. Mol. Spectrosc. **241**, 155 (2007).

[13] C. Henkel, K. M. Menten, M. T. Murphy, N. Jethava, V. V. Flambaum, J. A. Braatz, S. Muller, J. Ott, and R. Q. Mao, The density, the cosmic microwave background, and the proton-to-electron mass ratio in a cloud at redshift 0.9, Astron. Astrophys. **500**, 725 (2009).

[14] J. Bagdonaite, P. Jansen, C. Henkel, H. L. Bethlem, K. M. Menten, and W. Ubachs, A stringent limit on a drifting proton-to-electron mass ratio from alcohol in the early universe, Science **339**, 46 (2013).

[15] M. T. Murphy, V. V. Flambaum, S. Muller, and C. Henkel, Strong limit on a variable proton-to-electron mass ratio from molecules in the distant universe, Science **320**, 1611 (2008).

[16] N. Kanekar, Constraining changes in the proton-electron mass ratio with inversion and rotational lines, Astrophys. J. Lett. **728**, L12 (2011).

[17] D. A. Riechers, C. M. Bradford, D. L. Clements, C. D. Dowell, I. Pérez-Fournon, R. J. Ivison, C. Bridge, A. Conley, H. Fu, J. D. Vieira *et al.*, A dust-obscured massive maximum-starburst galaxy at a redshift of 6.34, Nature (London) **496**, 329 (2013).

[18] F. van Weerdenburg, M. T. Murphy, A. L. Malec, L. Kaper, and W. Ubachs, First constraint on cosmological variation of the proton-to-electron mass ratio from two independent telescopes, Phys. Rev. Lett. **106**, 180802 (2011).

[19] H. Rahmani, M. Wendt, R. Srianand, P. Noterdaeme, P. Petitjean, P. Molaro, J. B. Whitmore, M. T. Murphy, M. Centurion, H. Fathivavsari *et al.*, The UVES large program for testing fundamental physics - II. Constraints on a change in μ towards quasar HE 0027–1836, Mon. Not. R. Astron. Soc. **435**, 861 (2013).

[20] J. A. King, J. K. Webb, M. T. Murphy, and R. F. Carswell, Stringent Null Constraint on Cosmological Evolution of the Proton-to-Electron Mass Ratio, Phys. Rev. Lett. **101**, 251304 (2008).

[21] M. Wendt and P. Molaro, QSO 0347–383 and the invariance of m_p/m_e in the course of cosmic time, Astron. Astrophys. **541**, A69 (2012).

[22] C. Ledoux, P. Petitjean, and R. Srianand, Molecular hydrogen in a damped Lyα system at $z_{\rm abs} = 4.224$, Astrophys. J. Lett. **640**, L25 (2006).

[23] A. L. Malec, R. Buning, M. T. Murphy, N. Milutinovic, S. L. Ellison, J. X. Prochaska, L. Kaper, J. Tumlinson, R. F. Carswell, and W. Ubachs, Keck telescope constraint on cosmological variation of the proton-to-electron mass ratio, Mon. Not. R. Astron. Soc. **403**, 1541 (2010).

[24] J. Bagdonaite, W. Ubachs, M. T. Murphy, and J. B. Whitmore, Analysis of molecular hydrogen absorption toward QSO B0642–5038 for a varying proton-to-electron mass ratio, Astrophys. J. **782**, 10 (2014).

[25] See Supplemental Material at http://link.aps.org/supplemental/10.1103/PhysRevLett.114.071301 for the complete list of fitted transitions, the final fitted spectrum, and details on continuum fitting.

[26] Developed by R. F. Carswell *et al.*; available at http://www.ast.cam.ac.uk/ rfc/vpfit.html.

[27] M. T. Murphy, J. K. Webb, and V. V. Flambaum, Revision of VLT/UVES constraints on a varying fine-structure constant, Mon. Not. R. Astron. Soc. **384**, 1053 (2008).

[28] See Supplemental Material at http://link.aps.org/supplemental/10.1103/PhysRevLett.114.071301 for specific test results.

[29] Calculated via $\Delta\mu/\mu = 1/\Delta K_i \times \Delta v/c \times 1/\sqrt{n}$, where n is the number of ThAr transitions per one echelle order; typically $n > 15$.

[30] J. B. Whitmore, M. T. Murphy, and K. Griest, Wavelength calibration of the VLT-UVES spectrograph, Astrophys. J. **723**, 89 (2010).

[31] P. Molaro, S. A. Levshakov, S. Monai, M. Centurión, P. Bonifacio, S. D'Odorico, and L. Monaco, UVES radial velocity accuracy from asteroid observations. I. Implications for fine structure constant variability, Astron. Astrophys. **481**, 559 (2008).

[32] J. B. Whitmore and M. T. Murphy, Impact of instrumental systematic errors on fine-structure constant measurements with quasar spectra, Mon. Not. R. Astron. Soc. **447**, 446 (2015).

[33] http://archive.eso.org/eso/eso_archive_main.html.

[34] See Supplemental Material at http://link.aps.org/supplemental/10.1103/PhysRevLett.114.071301 for the observational details.

[35] http://kurucz.harvard.edu/sun/irradiance2005/irradthu.dat.

[36] To compute lookback times we adopt the following values of cosmological parameters: Hubble constant $H_0 = 67.3$ km/s/Mpc, $\Omega_{m,0} = 0.307$, $\Omega_{\Lambda,0} = 0.691$.

[37] S. A. Levshakov, F. Combes, F. Boone, I. I. Agafonova, D. Reimers, and M. G. Kozlov, An upper limit to the variation in the fundamental constants at redshift $z = 5.2$, Astron. Astrophys. **540**, L9 (2012).

[38] J. Bagdonaite, M. T. Murphy, L. Kaper, and W. Ubachs, Constraint on a variation of the proton-to-electron mass ratio from H_2 absorption towards quasar Q2348–011, Mon. Not. R. Astron. Soc. **421**, 419 (2012).

[39] J. A. King, M. T. Murphy, W. Ubachs, and J. K. Webb, New constraint on cosmological variation of the proton-to-electron mass ratio from Q0528–250, Mon. Not. R. Astron. Soc. **417**, 3010 (2011).

[40] R. I. Thompson, C. J. A. P. Martins, and P. E. Vielzeuf, Constraining cosmologies with fundamental constants - I. Quintessence and K-essence, Mon. Not. R. Astron. Soc. **428**, 2232 (2013).

[41] P. Brax, Environmental variation of constants in screened modified theories of gravity, Phys. Rev. D **90**, 023505 (2014).